A Film Bulk Acoustic Resonator Based on Ferroelectric Aluminum Scandium Nitride Films

Jialin Wang[®], Senior Member, IEEE, Mingyo Park[®], Senior Member, IEEE, Stefan Mertin, Tuomas Pensala, Member, IEEE, Farrokh Ayazi[®], Fellow, IEEE, and Azadeh Ansari[®], Member, IEEE

Abstract—This work reports on the first demonstration of the frequency tuning and intrinsic polarization switching of film bulk acoustic resonators (FBARs), based on sputtered AlScN piezoelectric thin films with Sc/(Al + Sc) ratio of approx. 30%. A box-like ferroelectric hysteresis behavior of 900 nm-thick Al_{0.7}Sc_{0.3}N sputtered films is obtained, showing a coercive electric field at ~3 MV/cm. The fundamental thickness-mode resonance of the bulk acoustic wave (BAW) resonator is measured at 3.17 GHz frequency with an excellent electromechanical coupling coefficient (k_t^2) of 18.1 %. The FBAR frequency response is studied, in both (i) the linear tuning regime, upon application of DC electric fields below the coercive field; as well as (ii) the polarization switching regime, upon application of electric fields above the coercive field. A large linear tuning range of 215 ppm $\times \mu$ m/V is obtained in case (i), resulting from the high scandium content. The series resonance frequency of the FBARs is switched ON and OFF in (ii) upon application of 350 V unipolar waveform across the Al_{0.7}Sc_{0.3}N thickness. This is the first demonstration of the intrinsically switchable AlN-based FBARs with a large tuning range; and record high k_t^2 reported for AlN-based FBARs to date. Furthermore, this work paves the way for realization of tunable and switchable wideband acoustic filters operating at [2020-0203] super high frequency ranges (SHF).

Index Terms—Ferroelectric, acoustic resonators, filters, fbar, aluminum scandium nitride, frequency tuning, piezoelectric films.

I. INTRODUCTION

THE evolution of mobile communication technologies has increased the demand for more frequency bands. Currently, a specific filter is required for each communication band, which leads to an increase in system complexity, size, and cost. Implementation of switchable and tunable acoustic filters has been proposed as one of the best solutions to

Manuscript received May 15, 2020; revised July 28, 2020; accepted August 1, 2020. Date of publication August 17, 2020; date of current version October 7, 2020. This work was supported in part by the National Science Foundation under Grant ECCS-1542174 and in part by the National Science Foundation CAREER Award under Grant ECCS-1944304. Subject Editor M. Rais-Zadeh. (Corresponding author: Jialin Wang.)

Jialin Wang, Mingyo Park, Farrokh Ayazi, and Azadeh Ansari are with the School of Electrical and Computer Engineering, Georgia Institute of Technology, Atlanta, GA 30332 USA (e-mail: jwang462@gatech.edu; m.park@gatech.edu; farrokh.ayazi@ece.gatech.edu; azadeh.ansari@ece.gatech.edu).

Stefan Mertin and Tuomas Pensala are with the VTT Technical Research Centre of Finland, 02044 Espoo, Finland (e-mail: stefan.mertin@vtt.fi; tuomas.pensala@vtt.fi).

Color versions of one or more of the figures in this article are available online at http://ieeexplore.ieee.org.

Digital Object Identifier 10.1109/JMEMS.2020.3014584

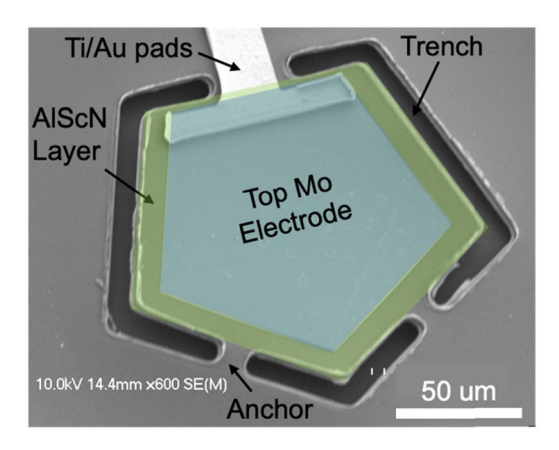
reduce the size and fabrication cost for the filter in mobile communication systems [1].

The quest for reconfigurable filters has invigorated research on various ferroelectric and paraelectric materials (e.g. PZT [2], [3], BST [4]) to realize switchable and tunable acoustic resonators. For example, in [2], the authors demonstrate a PZT-based FBAR with electromechanical coupling coefficient (k_t^2) of 7.3%, and quality factor (Q) of 85, and maximum tuning range of 2%. Reference [3] demonstrates a PZT-based FeCap based on COMS-MEMS resonator with Q of 656 and k_t^2 of 0.047%. Reference [5] demonstrates a BST based FBAR with k_t^2 and Q of 8.6% and 360, respectively.

The reported electromechanical coefficients have been severely limited for PZT-based FeCaps. Although PZT-based FBARs offer large electromechanical coupling factors, Q is limited especially at higher frequencies due to the associated losses at GHz frequencies [6]. PZT-based devices also suffer from CMOS incompatibility [7]. BST, on the other hand, requires DC field bias to switch ON (i.e. normally-off) [8]. Unlike PZT- and BST-based acoustic devices, AlN-based devices offer higher *Q factors* [9], low temperature coefficient of frequency (TCF) [10], and benefit from CMOS compatibility [11], high-frequency operation [10], as well as operation at high temperatures [4], [5], [12], [13]. However, AIN-based acoustic devices suffer from moderate k_t^2 (e.g. \sim 7% for FBARs [14]) and as a piezoelectric material, lacks intrinsic switching capability. Furthermore, a maximum frequency tuning range of 1.1% at \pm 200 V has been reported for AlN-based FBARs [9].

One solution that leads to enhancement of the electromechanical coupling and adds tuning/switching capability to AlN-based resonators is incorporation of scandium (Sc) into AlN films, particularly with Sc/(Al + Sc) ratios above 30%. The piezoelectric response is enhanced by increasing the Sc content [15], which leads to an increase in both k_t^2 [14], [16], and DC tunability [9]. Furthermore, the recent discovery of ferroelectric behavior in Aluminum Scandium Nitride (Al_{1-x}Sc_xN) thin films with x > 27% [17] can result in higher tuning ranges and added reconfigurability when used in arrays. This makes Al_{1-x}Sc_xN acoustic devices with x > 27% good candidates for RF wideband reconfigurable filters, by marrying the ferroelectric switching behavior with high k_t^2 . In this work, the ferroelectric behavior of an Al_{0.7}Sc_{0.3}N thin film is

1057-7157 © 2020 IEEE. Personal use is permitted, but republication/redistribution requires IEEE permission. See https://www.ieee.org/publications/rights/index.html for more information.



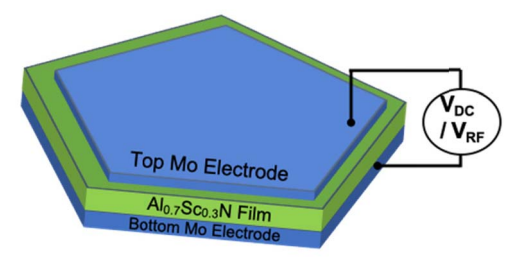


Fig. 1. (a) SEM image for the fabricated FBAR, (b) 3D schematic of the Mo (100 nm)/ AlScN (900 nm) / Mo (100 nm) stack studied under DC and RF voltage excitations in this work.

first characterized, showing a square-like polarization-electric field (P-E) loop, with coercive field and polarization intensity consistent with the data reported previously [17]. The linear tunability of the FBAR is studied with the applied DC bias below the coercive field (case (i)) with a measured k_t^2 of 18.1%, which is one of the highest k_t^2 values measured to date [14], [18]–[22], and mechanical quality factor (Q_m) above 300. The switching behavior of the FBAR is studied by measuring the admittance (Y_{11}) response of the FBAR before and after applied DC bias voltage above the coercive field (case (ii)). Fig. 1 shows the SEM image of the fabricated FBAR, along with the schematic of the FBAR, demonstrating the resonant stack and the measurement setup.

II. FABRICATION AND MEASUREMENT SETUP

A. Thin-Film Growth

The grown $Al_{0.7}Sc_{0.3}N$ thin-film layer has a thickness of 900 nm with 100 nm-thick top and bottom Molybdenum (Mo) electrode layers. The layer stack is sputter-deposited on a silicon-on-insulator (SOI) substrate at VTT Technical Research Centre of Finland, with a Von Ardenne CS 730S Cluster tool, achieving approx. 30% of Sc concentration and XRD rocking-curve full width half maximum (FWHM) close to 2 degrees, shown in Fig. 2(a). The SEM cross-section image of the sputtered $Al_{0.7}Sc_{0.3}N$ film is shown in Fig. 2(b), sandwiched between top and bottom Mo electrodes.

B. Fabrication Process

The detailed fabrication process is demonstrated in Fig. 3. The fabrication process starts with pattering the top Mo layer. Reactive Ion Etching (RIE) is used to etch the top Mo layer

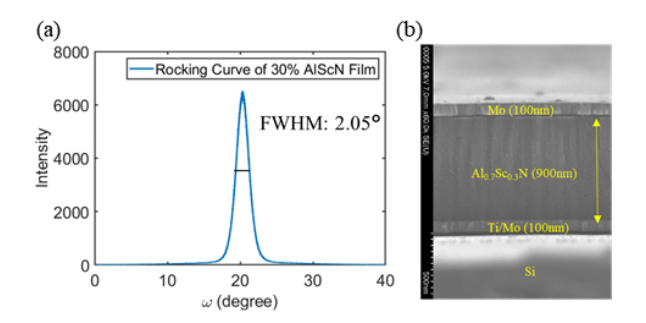


Fig. 2. (a) XRD rocking curve sputter-deposited Al_{0.7}Sc_{0.3}N on SOI substrate. (b) Cross-section SEM image of the resonant stack, indicating crystalline thin-film growth of both the Al_{0.7}Sc_{0.3}N thin film and the Mo electrode layers.

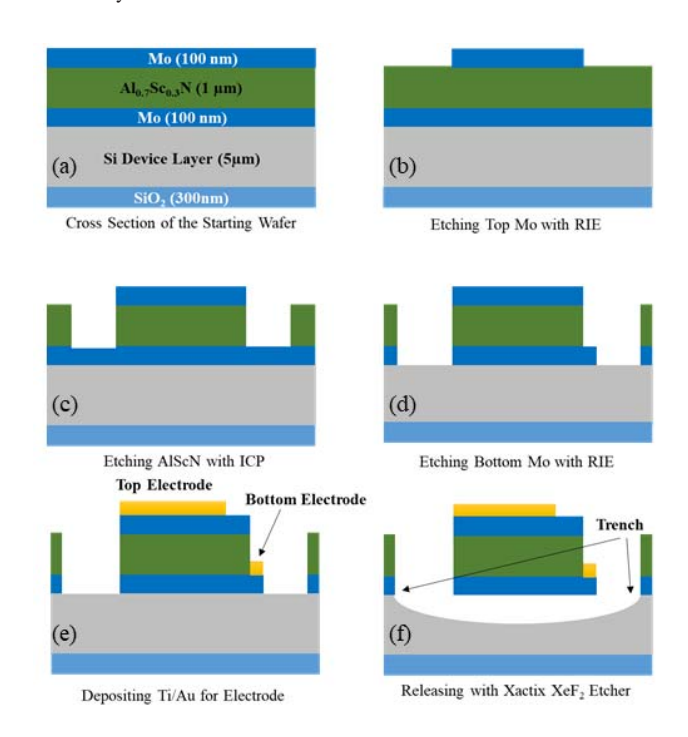


Fig. 3. AlScN FBAR fabrication process flow: (a) cross section of the starting wafer, (b) top Mo metal layer etching with reactive ion etching (RIE), (c) Al_{0.7}Sc_{0.3}N film etching with ICP, (d) bottom Mo metal layer etching with RIE, (e) deposition of Ti/Au electrical pad layers to contact the top and bottom electrodes, and finally (f) Si isotropic etching with xenon difluoride (XeF₂) for the FBAR device release.

with CF₄-based etchants (Fig. 3(b)). Al_{0.7}Sc_{0.3}N film is then patterned and etched with inductively coupled plasma (ICP) etching tool with Cl₂-based etchants (Fig. 3(c)). The bottom Mo layer is exposed after the ICP etching, which is subsequently patterned and etched (Fig. 3(d)). A stack of Ti/Au is then deposited onto the substrate to form metal contacts on both, top and bottom Mo, as shown in Fig 3(e). Finally, Fig. 3(f) shows the FBAR device released from the silicon device layer using Xactix xenon difluoride (XeF₂) isotropic etcher.

C. Measurement Setup

The hysteresis P-E loop of a fabricated Al_{0.7}Sc_{0.3}N metalferroelectric-metal (MFM) capacitor is measured using a modified S-T circuit (Fig. 4(a)) [23]. The ferroelectric capacitor

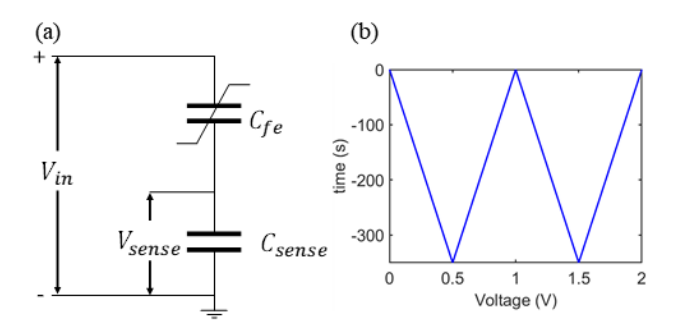


Fig. 4. (a) Schematic of the modified S-T circuit used for ferroelectric P-E loop measurement. (b) Unipolar waveform used in this work for switching the polarization of the ferroelectric film. A peak voltage of $\pm 350~V$ is applied across the 900 nm-thick $Al_{0.7}Sc_{0.3}N$ film, which is higher than the associated coercive field of 3 MV/cm.

has an area of $150 \times 150~\mu\text{m}^2$; resulting in an estimated value of 2.76 pF considering Al_{0.7}Sc_{0.3}N dielectric constant of 13.9 [24]. A commercial off-the-shelf sense capacitor of 680 pF is used, with an input signal of 300 V DC bias and a 2 kHz sinusoidal input. The P-E loop of the MFM capacitor is plotted in Fig. 5, by measuring the change in the voltage across the sensing capacitor according to (1).

$$P_{fe} = \frac{V_{sense} \times C_{sense}}{A_{fe}},\tag{1}$$

where P_{fe} (μ C/cm²) is the remnant polarization, V_{sense} is the measured voltage across the sensing capacitor, C_{sense} is the capacitance value of the sensing capacitor, and A_{fe} (cm²) is the area of the fabricated MFM capacitor.

The frequency response of the FBAR is measured with a Keysight N54244B PNA network analyzer. The performance of the low-voltage DC bias tuning of the FBAR is studied with the voltage potential applied to the FBAR during measurement ($V_{DC} + V_{RF}$). The DC bias (up to ± 80 V) is applied with a ZFBT-6GW+ BiasTee. The switching of the FBAR is achieved by applying a unipolar triangular wave (shown in Fig. 4(b)) with a peak voltage of -350 V at 1 kHz for 6 seconds. The FBAR could also be switched back by applying the same wave with the opposite peak voltage polarity (± 350 V). The frequency response is measured with the network analyzer of as-fabricated device (without any bias), and after positive and negative polarization switching.

III. RESULTS

A. Ferroelectric Hysteresis Behavior

Fig. 5 shows the hysteresis P-E loop measurement for the $Al_{0.7}Sc_{0.3}N$ thin-film. The box-like P-E loop shows the remnant polarization of the material reaches up to $80~\mu\text{C/cm}^2$ with a coercive field of 3 MV/cm. Compared to PZT, with $20~\mu\text{C/cm}^2$ of remnant polarization and a coercive field around 200~kV/cm [25], $Al_{0.7}Sc_{0.3}N$ ferroelectric films exhibit higher polarization and coercive fields, making them suitable materials for high power applications [17]. Unlike PZT, which exhibits a sloped P-E loop, caused by the leakage current [2], the perfect square P-E loop shown in Fig 5, is indicative of

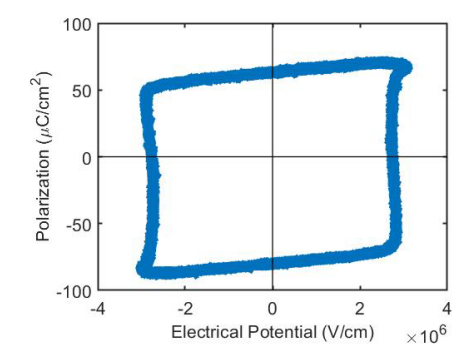


Fig. 5. The hysteresis P-E loop of the Al $_{0.7}$ Sc $_{0.3}$ N Capacitor with an area of 2.25×10^{-4} cm 2 and taken at an input frequency of 2 kHz.

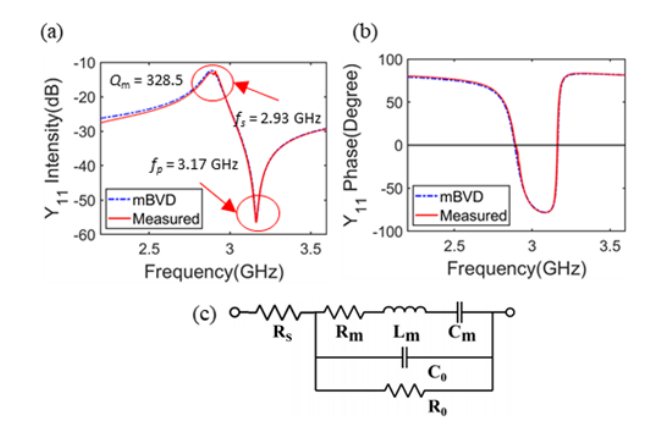


Fig. 6. (a) Measured and mBVD fitted plot for Al_{0.7}Sc_{0.3}N based FBAR, (b) phase of the measured and mBVD-fitted plot for Al_{0.7}Sc_{0.3}N based FBAR, and (c) modified Butterworth-Van Dyke (mBVD) circuit model.

excellent ferroelectric behavior of the Al_{0.7}Sc_{0.3}N films with low leakage currents.

B. Frequency Response of the Acoustic Resonators

The admittance of the measured FBAR device is shown in Fig. 6(a) and (b). The k_t^2 of 18.1% and Q_{bode} of 213 are evaluated by using equations (2) and (3) [26], where ω is the angular frequency (rad/s), and f_s / f_p are the series/parallel resonant frequencies.

$$Q_{bode} = \omega \times |S_{11}| \times \frac{group_{delay}(S_{11})}{1 - |S_{11}|^2}, \tag{2}$$

$$k_t^2 = \frac{\pi^2}{4} \times \frac{f_s(f_p - f_s)}{f_p^2}.$$
 [26]

The high k_t^2 of the FBAR is directly related to the enhanced piezoelectric performance with increased Sc content [27]. For AlScN films above 30% Sc/(Al/Sc) content the enhancement of the piezo coefficients is more than a factor 2.5 as compared to pure AlN films [15], [28]. The measured result is modeled with the modified Butterworth-Van Dyke (mBVD) model with the circuit shown in Fig. 6(c). The mBVD model consists of the motional branch, which is modeled with R_m , C_m , and L_m , and the electrical branch, consisting of R_o and C_o . The fitted components are shown in Table I with the unloaded quality

 $\begin{array}{c} \text{TABLE I} \\ \text{MBVD Model Parameter} \end{array}$

mB\ Mod			C _m (fF)	L _m (nH)	Co (fF)	Ro (Ω)	k_t^2 (%)	Qm
Valu	ie 3.6	6 0.34	488	6.09	2660	2225	18.1	328.5

TABLE II

COMPARISON OF ELECTRICAL MECHANICAL COUPLING COEFFICIENT
AND QUALITY FACTOR WITH PERVIOUS WORK

Material	k_t^2 (%)	Q_{Bode} factor
AlN [14]	6.16	739
Al _{0.91} Sc _{0.09} N [14]	9.53	513
Al _{0.85} Sc _{0.15} N [14]	12.00	348
$Al_{0.59}Sc_{0.41}N$ [22]	19.0	=
SiO_2+	7.9	-
$Al_{0.59}Sc_{0.41}N$ [18]		
Diamond+	2.4	700
$Al_{0.59}Sc_{0.41}N$ [18]		
Al _{0.59} Sc _{0.41} N [19]	12	=
Al _{0.65} Sc _{0.35} N [20]	15.5	=
Al _{0.73} Sc _{0.27} N [21]	12.18	178.8
Al _{0.7} Sc _{0.3} N*	18.1	210
[This Work]		

factor (Q_m) of the resonator obtained using (4). The measured data and fitted mBVD model are shown in Fig. 6 (a) and (b).

$$Q_m = \frac{1}{R_m} \sqrt{\frac{L_m}{C_m}} \tag{4}$$

Table II shows the comparison of k_t^2 and Q_{bode} of the fabricated FBAR in this work and prior work, highlighting that this work exhibits one of the highest k_t^2 values published to date.

C. Analog Frequency Tuning With Applied Electric Fields Below the Coercive Field

The DC electric field bias below the coercive field will induce a linear change in both the parallel and the series resonant frequencies (Fig. 7). The measured f_s of the FBAR is at 2.93 GHz at zero bias. When bias voltages of positive/ negative 80 V DC are applied across the thickness of the FBAR, together with the RF excitation signal, f_s shifts to 2.916/2.95 GHz, respectively, resulting in 239 ppm $\times \mu$ m/V of tuning range. With the same method, the tunability of f_p is calculated to be around 150 ppm $\times \mu m$ /V. The difference of tunability between f_s and f_p is caused by the slight shift in k_t^2 since the DC bias may induce stress in the thin film [9]. The change in the parallel and series resonant frequencies are plotted in Fig. 7 (b), showing a linear frequency tuning vs. DC voltage at -80 V to 80 V bias voltages. The overall tunability of the resonant frequency is about 1.17%, which is calculated with the frequency between ± 80 V DC bias. With ±200 V DC bias, the tunability of Al_{0.7}Sc_{0.3}N based FBAR could achieve up to 2.9%, which is about 2.6 times higher compared to AlN based FBARs with typical tunability range of \sim 1.1% or 54 ppm $\times \mu$ m/V with \pm 200 V DC bias applied [9].

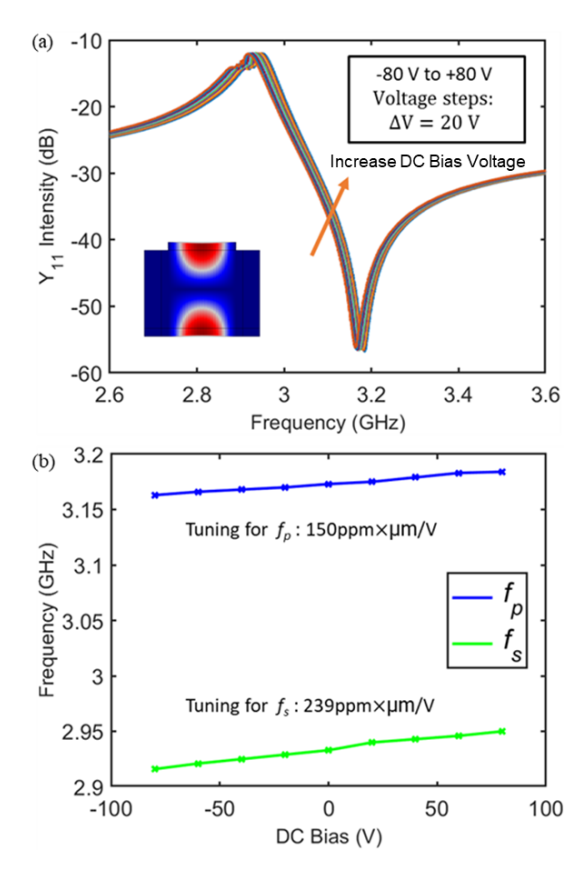


Fig. 7. (a) Magnitude of Y_{11} plot of the low DC bias response for the fabricated $Al_{0.7}Sc_{0.3}N$ based FBAR with DC bias (-80 V to 80 V) below the measured coercive field of the $Al_{0.7}Sc_{0.3}N$ thin film. The COMSOL simulation of displacement mode shape at the fundamental thickness-extensional resonance is shown in the inset. The red and blue colors in the cross section simulation correspond to the maximum and minimum displacement amplitude respectively. (b) Frequency (f_s and f_p) vs. DC voltage plot of the fabricated FBARs with DC bias voltages below the coercive voltage.

In the linear tuning regime, the anti-resonant frequency (f_a) is:

$$f_a = \frac{1}{2t} \sqrt{\frac{c^D}{\rho}},\tag{5}$$

where t is the thickness of the piezoelectric film, c^D the stiffness coefficient at constant D, D the constant electric displacement, and ρ the density of the material. Since the FBAR operates in the thickness-extensional mode, c_{33} value is used as c^D in (5) to calculate the resonance frequency. The change in the stiffness coefficient and the anti-resonant frequency coefficient, f_a is linearly proportional to the piezoelectric coefficient of the material, d_{33} , with the relationship shown in (6) [9], where U is the DC bias voltage applied to the two electrodes.

$$\frac{dc_{33}^D}{c_{33}^D} = -d_{33}\frac{U}{t} + 2\frac{df_a}{f_a} \tag{6}$$

Eq. (7) could be derived out by rearranging (5) and (6), which shows parallel anti-resonant frequency is solely dependent on the piezoelectric coefficient of the material with DC tuning. The tunability for series resonant frequency can be extracted from f_a and k_t^2 tuning. Since the piezoelectric coefficient increases as the Sc concentration increases in

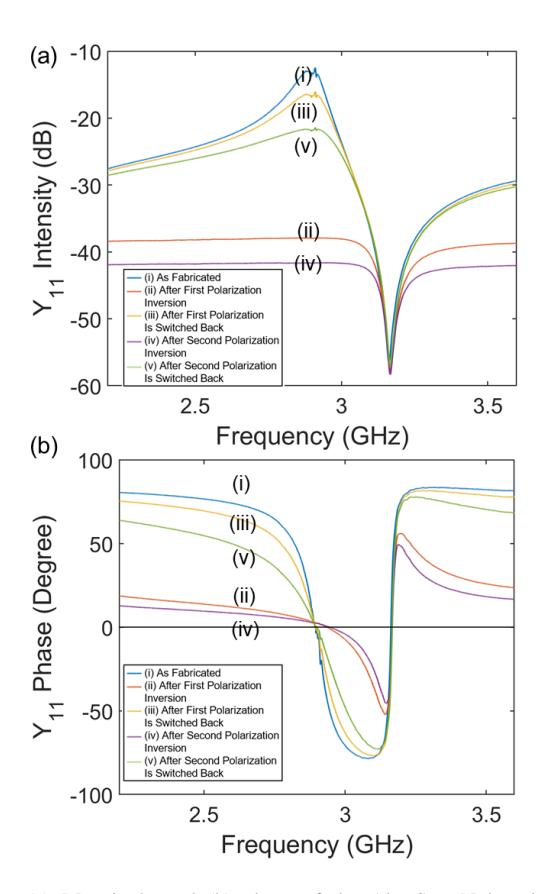


Fig. 8. (a) Magnitude and (b) phase of the $Al_{0.7}Sc_{0.3}N$ based FBAR admittance (Y_{11}) over multiple switching cycles, showing the response of as-fabricated device, and after positive bias and negative voltage biases are applied sequentially for t = 6s for each switching. The sequence is marked with (i)-(v).

AlScN films [14], [24], [28], the Al_{0.7}Sc_{0.3}N based FBARs will offer larger tuning capabilities compared to AlN based FBAR devices.

$$\frac{df_a^2}{f_a^2} = -d_{33}\frac{U}{t} + 2\frac{df_a}{f_a} \tag{7}$$

D. Switching Behavior With Applied Electric Fields Above the Coercive Field

Fig. 8 shows the Y_{11} plot of the FBAR frequency response in five sequential steps. First, the as-fabricated device is measured without application of any DC bias voltage, (i). Secondly, the polarization is inverted upon application and removal of a negative unipolar switching voltage, ((ii) first polarization inversion). Thirdly, AlScN polarization is switched back to N-polar [17], upon application and removal of a positive unipolar voltage, (iii). Finally, the last two steps are repeated, switching the film polarization back to Al-, (iv) and N-, (v) polar. The FBAR response could switch between two distinct states, which are shown in both the Y_{11} magnitude and phase (Fig. 8). The k_t^2 , Q_{Bode} and Q_m (unloaded Q) of the as-fabricated FBAR, are calculated using (1), (2) and (4), as 18.1%, 213 and 328, respectively. The Q degradation after multiple polarization switchings (i.e. state (iii) and (v) compared to state (i)) is caused by the fatigue built up in the thin film due to the large poling voltage during different

switching cycles [29]. The series resonance frequency (f_s) of the FBAR disappears after the negative switching bias is applied and then removed [30]. This rather interesting switching mechanism is observed when the unipolar bias voltage shown in Fig. 4(b) is applied for a duration time (t) greater than 3 seconds (t > 3 s). The FBAR series resonance peak switching is attributed to the resistance switching at the two polarization states, similar to resistive switching observed in other MFM capacitors [31]–[35].

The MFM capacitor can be modelled as a series resistor (R_s), representing the electrical resistance of the metal electrodes and the resistance of metal electrode/ferroelectric material interface; and a parallel ferroelectric resistance (R_{FE}) and capacitance (C_{FE}), represented as R₀ and C₀ in the mBVD model in Fig. 6(c). Switching the polarization of Mo/AlScN/Mo films, not only switches the polarity of e₃₃ piezoelectric coefficient, but can also cause a change in R_s, R_{FE}, and C_{FE} depending on the applied stress. It has been shown that an increase in the energy barrier height of metal/ferroelectric interface can lead to an increase in the series resistance (R_s) [33], [35]. In particular, [32] reports on a study of the space-charge effect on the series film resistance in MFM capacitors, showing a 1000% increase in film resistance after polarization switching. Detailed discussions of the dynamics of ferroelectric polarization switching requires in-depth material characterization, which is a subject of future work.

IV. CONCLUSION

This work demonstrated the first switchable Al_{0.7}Sc_{0.3}Nbased FBAR utilizing the newly discovered ferroelectric behavior of $Al_{1-x}Sc_xN$ thin films, with x = 30%. The hysteresis P-E measurement is reported, showing a high remnant polarization of Al_{0.7}Sc_{0.3}N MFM (Metal-Ferroelectric-Metal) capacitors, along with a high coercive field. The analog frequency tuning of the fundamental thickness-extensional resonance mode of the FBAR devices is studied with DC bias and RF signal applied with a Bias Tee, showing a large tuning range. A record high effective electromechanical coupling coefficient (k_t^2) of the fabricated FBAR is measured as 18.1%, thanks to the high Sc content [14], [18]-[22]. Furthermore, the switching behavior of the Al_{0.7}Sc_{0.3}N-based FBARs was studied upon application and removal of unipolar triangle waveforms with a peak voltage of ± 350 V, which could then be switched back by applying an equal and opposite polarity voltage bias. The high k_t^2 , high operating frequency, and tuning/switching behavior of the Al_{0.7}Sc_{0.3}N based FBARs make it a promising candidate as the building block for tunable and switchable wideband acoustic filters operating in SHF ranges.

ACKNOWLEDGMENT

The sputtered piezo-stack Mo/Al_{0.7}Sc_{0.3}N/Mo was provided by VTT Technical Research Centre of Finland. The FBAR devices were fabricated at the Institute for Electronics and Nanotechnology (IEN) cleanroom facility at the Georgia Institute of Technology, a member of the National Nanotechnology Coordinated Infrastructure (NNCI).

REFERENCES

- S. Gevorgian, A. Tagantsev, and A. Vorobiev, "Introduction," in *Tuneable Film Bulk Acoustic Wave Resonators* (Engineering Material and Processes). London, U.K.: Springer, 2013, pp. 1–15, doi: 10.1007/978-1-4471-4944-6
- [2] C. Zinck, E. Defay, A. Volatier, G. Caruyer, D. P. Tanon, and L. Figuiere, "Design, integration and characterization of PZT tunable FBAR," in Proc. 14th IEEE Int. Symp. Appl. Ferroelectr. (ISAF), Montreal, QC, Canada, Aug. 2004, pp. 29–32, doi: 10.1109/ISAF.2004.1418330.
- [3] Y. He, B. Bahr, M. Si, P. Ye, and D. Weinstein, "Switchable mechanical resonance induced by hysteretic piezoelectricity in ferroelectric capacitors," in *Proc. 20th Int. Conf. Solid-State Sens.*, Actuators Microsyst. Eurosensors XXXIII (TRANSDUCERS EUROSENSORS XXXIII), Berlin, Germany, Jun. 2019, pp. 717–720, doi: 10.1109/TRANSDUCERS.2019. 8808623.
- [4] S. Lee, V. Lee, S. A. Sis, and A. Mortazawi, "Linearity analysis of intrinsically switchable ferroelectric FBAR filters," in *IEEE MTT-S Int. Microw. Symp. Dig.*, Seattle, WA, USA, Jun. 2013, pp. 1–3, doi: 10. 1109/MWSYM.2013.6697782.
- [5] M. Z. Koohi and A. Mortazawi, "Reconfigurable radios employing ferroelectrics: Recent progress on reconfigurable RF acoustic devices based on thin-film ferroelectric barium strontium titanate," *IEEE Microw. Mag.*, vol. 21, no. 5, pp. 120–135, May 2020, doi: 10.1109/MMM.2020. 2971376
- [6] J. D. Larson, S. R. Gilbert, and B. Xu, "PZT material properties at UHF and microwave frequencies derived from FBAR measurements," in *Proc. IEEE Ultrason. Symp.*, Montreal, QC, Canada, vol. 1, Aug. 2004, pp. 173–177, doi: 10.1109/ULTSYM.2004.1417696.
- [7] Q. Su et al., "Self-separated PZT thick films with bulk-like piezoelectric and electromechanical properties," J. Mater. Res., vol. 26, no. 11, pp. 1431–1435, Jun. 2011, doi: 10.1557/jmr.2011.115.
- [8] M. Z. Koohi and A. Mortazawi, "Negative piezoelectric based electric-field-actuated mode-switchable multilayer ferroelectric FBARs for selective control of harmonic resonances without degrading k2eff," *IEEE Trans. Ultrason., Ferroelectr., Freq. Control*, early access, Apr. 20, 2020, doi: 10.1109/TUFFC.2020.2988632.
- [9] E. Defaÿ, N. B. Hassine, P. Emery, G. Parat, J. Abergel, and A. Devos, "Tunability of alluminum nitride acoustic resonators: A phenomenological approach," *IEEE Trans. Ultrason., Ferroelectr., Freq. Control*, vol. 58, no. 12, pp. 2516–2520, Dec. 2011, doi: 10.1109/TUFFC.2011. 2114.
- [10] A. Ansari, "Single crystalline scandium aluminum nitride: An emerging material for 5G acoustic filters," in *IEEE MTT-S Int. Microw. Symp. Dig.*, Guangzhou, China, May 2019, pp. 1–3, doi: 10.1109/IEEE-IWS.2019. 8804148
- [11] M. H. S. Alrashdan, A. A. Hamzah, B. Y. Majlis, and M. F. Aziz, "Aluminum nitride thin film deposition using DC sputtering," in *Proc. IEEE Int. Conf. Semiconductor Electron. (ICSE)*, Kuala Lumpur, Malaysia, Aug. 2014, pp. 72–75, doi: 10.1109/SMELEC.2014.6920798.
- [12] S. Gevorgian and A. Vorobiev, "Tunable FBARs: Intrinsic vs. Extrinsic tunability," in *IEEE MTT-S Int. Microw. Symp. Dig.*, Montreal, QC, Canada, Jun. 2012, pp. 1–3, doi: 10.1109/MWSYM.2012.6258382.
- [13] M.-H. Park and S.-H. Kim, "Thermal conductivity of AlN thin films deposited by RF magnetron sputtering," *Mater. Sci. Semicond. Process.*, vol. 15, no. 1, pp. 6–10, Feb. 2012, doi: 10.1016/j.mssp.2011.04.007.
- [14] M. Moreira, J. Bjurström, I. Katardjev, and V. Yantchev, "Aluminum scandium nitride thin-film bulk acoustic resonators for wide band applications," *Vaccum*, vol. 86, nos. 1–4, pp. 23–36, Jul. 2011, doi: 10.1016/j. vacuum.2011.03.026.
- [15] M. A. Caro et al., "Erratum: Piezoelectric coefficients and spontaneous polarization of ScAlN (2015 J. Phys. Condens. Matter 27 245901)," J. Phys., Condens. Matter, vol. 27, no. 27, Jul. 2015, Art. no. 279602, doi: 10.1088/0953-8984/27/27/279602.
- [16] M. Park, Z. Hao, R. Dargis, A. Clark, and A. Ansari, "Epitaxial aluminum scandium nitride super high frequency acoustic resonators," *J. Microelectromech. Syst.*, vol. 29, no. 4, pp. 490–498, Aug. 2020, doi: 10.1109/JMEMS.2020.3001233.
- [17] S. Fichtner, N. Wolff, F. Lofink, L. Kienle, and B. Wagner, "AlScN: A III-V semiconductor based ferroelectric," J. Appl. Phys., vol. 125, no. 11, Mar. 2019, Art. no. 114103, doi: 10.1063/1.5084945.
- [18] H. Igeta, M. Totsuka, M. Suzuki, and T. Yanagitani, "Temperature characteristics of ScAlN/SiO₂ BAW resonators," in *Proc. IEEE Int. Ultrason. Symp. (IUS)*, Kobe, Japan, Oct. 2018, pp. 1–4, doi: 10.1109/ULTSYM. 2018.8580165.

- [19] T. Yanagitani and M. Suzuki, "Electromechanical coupling and gigahertz elastic properties of ScAIN films near phase boundary," *Appl. Phys. Lett.*, vol. 105, no. 12, Sep. 2014, Art. no. 122907, doi: 10.1063/1.4896262.
- [20] K. Umeda, H. Kawai, A. Honda, M. Akiyama, T. Kato, and T. Fukura, "Piezoelectric properties of ScAlN thin films for piezo-MEMS devices," in *Proc. IEEE 26th Int. Conf. Micro Electro Mech. Syst. (MEMS)*, Taipei, Taiwan, Jan. 2013, pp. 733–736, doi: 10.1109/MEMSYS.2013.6474347.
- [21] M. Schneider, M. DeMiguel-Ramos, A. J. Flewitt, E. Iborra, and U. Schmid, "Scandium aluminium nitride-based film bulk acoustic resonators," *Proceedings*, vol. 1, no. 4, p. 305, 2017, doi: 10.3390/ proceedings1040305.
- [22] K.-H. Sano, R. Karasawa, and T. Yanagitani, "High electromechanical coefficient kt2=19% thick ScAlN piezoelectric films for ultrasonic transducer in low frequency of 80 MHz," in *Proc. IEEE Int. Ultrason. Symp. (IUS)*, Washington, DC, USA, Sep. 2017, pp. 1–4, doi: 10.1109/ ULTSYM.2017.8092005.
- [23] C. B. Sawyer and C. H. Tower, "Rochelle salt as a dielectric," *Phys. Rev.*, vol. 35, no. 3, pp. 269–273, Feb. 1930.
- [24] M. Akiyama, K. Umeda, A. Honda, and T. Nagase, "Influence of scandium concentration on power generation figure of merit of scandium aluminum nitride thin films," *Appl. Phys. Lett.*, vol. 102, no. 2, Jan. 2013, Art. no. 021915, doi: 10.1063/1.4788728.
- [25] P. Panda and B. Sahoo, "PZT to lead free piezo ceramics: A review," Ferroelectrics, vol. 474, no. 1, pp. 128–143, 2015, doi: 10.1080/00150193. 2015.997146.
- [26] H. Campanella, "Characterization techniques," in Acoustic Wave and Electromechanical Resonators: Concept to Key Applications. Boston, MA, USA: Artech House, 2010, pp. 127–158.
- [27] S. Gevorgian, A. Tagantsev, and A. Vorobiev, "Models of FBARs," in Tuneable Film Bulk Acoustic Wave Resonators (Engineering Material and Processes). London, U.K.: Springer, 2013, pp. 55–88, doi: 10.1007/ 978-1-4471-4944-6 3.
- [28] S. Mertin et al., "Enhanced piezoelectric properties of c-axis textured aluminium scandium nitride thin films with high scandium content: Influence of intrinsic stress and sputtering parameters," in Proc. IEEE Int. Ultrason. Symp. (IUS), Sep. 2017, pp. 1–4, doi: 10.1109/ULTSYM. 2017.8092187.
- [29] Y. A. Genenko, J. Glaum, M. J. Hoffmann, and K. Albe, "Mechanisms of aging and fatigue in ferroelectrics," *Mater. Sci. Eng.*, B, vol. 192, pp. 52–82, Feb. 2015.
- [30] J. Wang, M. Park, S. Mertin, T. Pensala, F. Ayazi, and A. Ansari, "A high-kt² switchable ferroelectric Al_{0.7}Sc_{0.3}N film bulk acoustic resonator," in *Proc. IEEE Int. Freq. Control Symp. (IFCS)*, to be published.
- [31] Z. B. Yan and J.-M. Liu, "Resistance switching memory in perovskite oxides," *Ann. Phys.*, vol. 358, pp. 206–224, Jul. 2015, doi: 10.1016/j. aop.2015.03.028.
- [32] B. B. Tian et al., "Space-charge effect on electroresistance in metalferroelectric-metal capacitors," Sci. Rep., vol. 5, no. 1, pp. 1–9, Nov. 2016, doi: 10.1038/srep18297.
- [33] P. Lopez-Varo et al., "Physical aspects of ferroelectric semiconductors for photovoltaic solar energy conversion," *Phys. Rep.*, vol. 653, pp. 1–40, Oct. 2016, doi: 10.1016/j.physrep.2016.07.006.
- [34] R. Meyer, J. R. Contreras, A. Petraru, and H. Kohlstedt, "On a novel ferro resistive random access memory (FRRAM): Basic model and first experiments," *Integr. Ferroelectr.*, vol. 64, no. 1, pp. 77–88, Jan. 2004, doi: 10.1080/10584580490893655.
- [35] J. E. Rault et al., "Interface electronic structure in a metal/ferroelectric heterostructure under applied bias," Phys. Rev. B, Condens. Matter, vol. 87, no. 15, Apr. 2013, doi: 10.1103/PhysRevB.87.155146.



Jialin Wang (Senior Member, IEEE) received the B.S. and M.S. degrees from the Georgia Institute of Technology, Atlanta, GA, USA, in 2017 and 2019, respectively, where he is currently pursuing the Ph.D. degree with the School of Electrical and Computer Engineering. His current research interests include the design and fabrication of III–V compound semiconductor MEMS resonators and filters.



Mingyo Park (Senior Member, IEEE) received the B.S. and M.S. degrees in electrical and electronic engineering from Yonsei University, Seoul, South Korea, in 2014 and 2016, respectively. She is currently pursuing the Ph.D. degree with the Department of Electrical and Computer Engineering, Georgia Institute of Technology, Atlanta, GA, USA. Her research interests include phononic frequency combs and RF MEMS resonators and filters for super high-frequency (SHF) range applications. She was a recipient of the LG Display Education Scholarship in 2016.



Stefan Mertin studied physics from the Ruprecht Karl University of Heidelberg, Germany. He received the Ph.D. degree from the EPFL (Swiss Federal Institute of Technology), Lausanne, Switzerland, in 2015, with focus on ultra-high vacuum systems and sputtering technology. During his Ph.D. thesis, he developed new thin-film materials by co-sputtering and designed multi-layered optical thin-film filters for solar applications. From 2015 to 2017, he worked as a Post-Doctoral Researcher with the Ceramics Laboratory and the

Electroceramic Thin Films Group, Materials Science Institute, EPFL, where he focused on piezo-electrical and structural characterisation (XRD, SEM, and TEM) of sputtered scandium doped aluminium nitride (ScAlN) thin films. He is currently working with the VTT Technical Research Centre of Finland as Senior Process Engineer, being responsible for the sputter thin-film deposition technology at VTT's Micronova Nanofabrication Centre. His research interests include piezoelectric thin-film process development and material characterisation with focus on high Sc containing ScAlN thin films for MEMS resonators and pMUTs.



Tuomas Pensala (Member, IEEE) was born in Helsinki, Finland, in 1972. He received the degree in engineering physics from the Helsinki University of Technology in 2000 and the D.Sc. (Tech.) degree in applied physics from Aalto University in 2011. He has been with the VTT Technical Research Centre of Finland since 1998, where he currently holds a position of principal scientist. He has authored and coauthored more than 50 scientific articles and presentations on thin film, RF and MEMS devices, and contributed to more than 20 patent families. His

research interests included microacoustic RF filters, MEMS and PiezoMEMS resonators and sensors, and thin film technology.



Farrokh Ayazi (Fellow, IEEE) received the B.S. degree in electrical engineering from the University of Tehran, Iran, in 1994, and the M.S. and Ph.D. degrees in electrical engineering from the University of Michigan, Ann Arbor, in 1997 and 2000, respectively. He was the Co-Founder and the CTO of Qualtreì, a spin-out of his research laboratory that commercialized bulk acoustic-wave silicon gyroscopes for high-precision applications, which was acquired by Panasonic in 2016. He is currently the Ken Byers Professor of microsystems

with the School of Electrical and Computer Engineering, Georgia Institute of Technology, Atlanta, GA, USA. He has authored over 250 refereed technical and scientific articles and holds 55 patents. His main research interest includes integrated micro/nano-electro-mechanical-systems, with a focus on resonators and inertial sensors. He was the General Chair of the IEEE Micro-Electro-Mechanical-Systems Conference in 2014, San Francisco, CA, USA. He is an Editor of the IEEE Transactions on Electron Devices and Sensors and Actuators A: Physical (Elsevier) and a past Editor of the IEEE/ASME JOURNAL OF MICROELECTROMECHANICAL SYSTEMS.



Azadeh Ansari (Member, IEEE) received the B.S. degree in electrical engineering from the Sharif University of Technology, Tehran, Iran, in 2010, and the M.S. and Ph.D. degrees in electrical engineering from the University of Michigan, Ann Arbor, in 2013 and 2016, respectively, focusing upon III–V semiconductor and MEMS devices and microsystems for RF applications. She is currently the Sutterfield family Assistant Professor with the School of Electrical and Computer Engineering, Georgia Institute of Technology. Prior to joining

the ECE Faculty, she was a Post-Doctoral Scholar with the Department of Physics, California Institute of Technology. Her research interests include nano/micro electromechanical systems (N/MEMS) and radio frequency (RF) integrated systems. She was a recipient of the 2019 NSF CAREER Award and the 2017 ProQuest Distinguished Dissertation Award from the University of Michigan. She received the University of Michigan Richard and Eleanor Towner Prize for Outstanding Ph.D. research in 2016.